31291-31302. 2009.

Nakagami A, Negishi T, Kawasaki K, Imai N, Nishida Y, Ihara T, Kuroda Y, Yoshikawa Y, Koyama T. Alterations in male infant behaviors towards its mother by prenatal exposure to bisphenol A in cynomolgus monkeys (Macaca fascicularis) during early suckling period. ***Psychoneuroendocrinology.*** 34: 1189-1197. 2009.

2. 学会発表

根岸隆之、高橋理貴、小柳洸志、大西大空、平野靖史郎、田代朋子. 小脳顆粒細胞におけるジフェニルアルシン酸による酸化ストレスと細胞死. 第 52 回日本神経化学会. 群馬県伊香保. 2009 年 6 月 22 日.

小柳洸志、高橋理貴、根岸隆之、田代朋子. 培養小脳顆粒細胞における低カリウム誘発細胞死に対する甲状腺ホルモン T4 の細胞保護作用. 第 52 回日本神経化学会. 群馬県伊香保. 2009 年 6 月 22 日.

角田正史、若佐美佳、浅川秀雄、高橋理貴、根岸隆之、峡戸孝也、細川まゆ子、菅谷ちえ美、井上葉子、相澤好治、田代朋子. ラット脳の発達に対するトリブチルスズ曝露の影響に関する二世代トキシコジェノミック研究. 第 52 回日本神経化学会.群馬県伊香保. 2009 年 6 月 24 日.

澤野恵梨香、高橋理貴、船津尚子、木村洋人、根岸隆之、田代朋子. GABA 神経伝達機構の発達における甲状腺ホルモンの役割. 第 52 回日本神経化学会.群馬県伊香保. 2009 年 6 月 22 日.

宇野健史、石橋瑛、高橋理貴、根岸隆之、田代朋子. 2 型糖尿病モデル・GK ラットの脳におけるホモシステイン代謝の変化. 第 52 回日本神経化学会. 群馬県伊香保. 2009 年 6 月 22 日.

根岸隆之. サル類の行動を指標とした胎生期化学物質曝露による神経発達毒性の評価. 日本先天異常学会（DNT 講演）. 鹿児島県鹿児島市. 2009 年 6 月 25 日.

H. 知的財産権の出願・登録状況

なし

Fig. 1

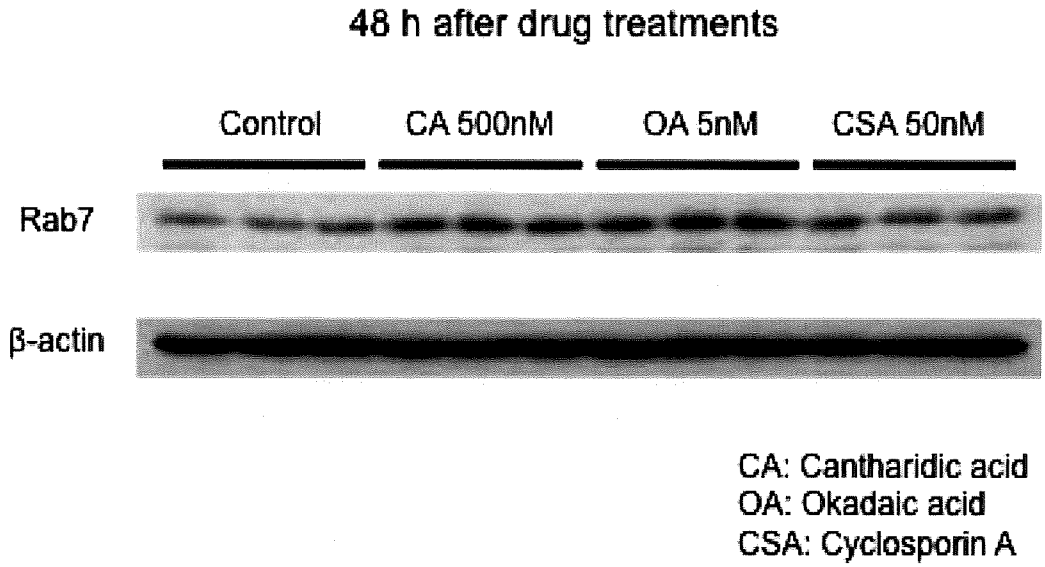

CA: Cantharidic acid
OA: Okadaic acid
CSA: Cyclosporin A

IV. 研究成果の刊行に関する一覧表

研究成果の刊行に関する一覧表

雑誌

発表者氏名	論文タイトル名	発表誌名	巻号	ページ	出版年
Kimura N, Inoue M, Okabayashi S, Ono F, Negishi T.	Dynein dysfunction induces endocytic pathology accompanied by an increase in Rab GTPases: a potential mechanism underlying age-dependent endocytic dysfunction.	J Biol Chem	284(45)	31291-31302	2009
Kimura N.	Endocytic dysfunction and Alzheimer's disease.	Endocytosis (book)	In Press		
Asakawa H, Tsunoda M, Kaido T, Hosokawa M, Sugaya C, Inoue Y, Kudo Y, Satoh T, Katagiri H, Akita H, Saji M, Wakasa M, Negishi T, Tashiro T, Aizawa Y.	Enhanced Inhibitory Effects of TBT Chloride on the Development of F(1) Rats.	Arch Environ Contam Toxicol	In Press		
Nakagami A, Negishi T, Kawasaki K, Imai N, Nishida Y, Ihara T, Kuroda Y, Yoshikawa Y, Koyama T.	Alterations in male infant behaviors towards its mother by prenatal exposure to bisphenol A in cynomolgus monkeys (Macaca fascicularis) during early suckling period.	Psychoneuroendocrinology	34	1189-1197	2009

Okabayashi S and Kimura N.	Leucine-rich glioma inactivated 3 is involved in amyloid β peptide uptake by astrocytes and endocytosis itself.	Neuroreport.	19(12)	1175-1179	2008
Kobayashi Y, Negishi T, Mizumura A, Watanabe T, Hirano S.	Distribution and excretion of arsenic in cynomolgus monkey following repeated administration of diphenylarsinic acid.	Arch Toxicol	82(8):	553-561.	2008
Takahashi M, Negishi T, Imamura M, Sawano E, Kuroda Y, Yoshikawa Y, Tashiro T.	Alterations in gene expression of glutamate receptors and exocytosis-related factors by a hydroxylated-polychlorinated biphenyl in the developing rat brain.	Toxicology	257(1-2):	17-24	2009

V. 研究成果の刊行物・別刷

THE JOURNAL OF BIOLOGICAL CHEMISTRY VOL. 284, NO. 45, pp. 31291–31302, November 6, 2009

Dynein Dysfunction Induces Endocytic Pathology Accompanied by an Increase in Rab GTPases

A POTENTIAL MECHANISM UNDERLYING AGE-DEPENDENT ENDOCYTIC DYSFUNCTION[*][S]

Received for publication, April 23, 2009, and in revised form, September 12, 2009 Published, JBC Papers in Press, September 15, 2009, DOI 10.1074/jbc.M109.012625

Nobuyuki Kimura[‡1], **Makoto Inoue**[§], **Sachi Okabayashi**[‡¶], **Fumiko Ono**[‡¶], **and Takayuki Negishi**[‖]

From the [‡]*Laboratory of Disease Control, Tsukuba Primate Research Center, National Institute of Biomedical Innovation, 1-1 Hachimandai, Tsukuba-shi, Ibaraki 305-0843,* [§]*DNAVEC Research Inc., 1-25-11 Kannondai, Tsukuba-shi, Ibaraki 305-8421* [¶]*The Corporation for Production and Research of Laboratory Primates, 1 Hachimandai, Tsukuba-shi, Ibaraki 305-0843, and the* [‖]*Department of Chemistry and Biological Science, School of Science and Engineering, Aoyama Gakuin University, 5-10-1 Fuchinobe, Sagamihara-shi, Kanagawa 229-8558, Japan*

Growing evidence suggests that endocytic dysfunction is intimately involved in early stage Alzheimer disease pathology, such as the accumulation of β-amyloid precursor protein in enlarged early endosomes. However, it remains unclear how endocytic dysfunction is induced in an age-dependent manner. Cytoplasmic dynein, a microtubule-based motor protein, interacts with another microtubule-associated protein, dynactin. The resulting dynein-dynactin complex mediates minus end-directed vesicle transport, including endosome trafficking. We have previously shown that the interaction between dynein-dynactin complexes is clearly attenuated in aged monkey brains, suggesting that dynein-mediated transport dysfunction exists in aged brains. Our immunohistochemical analyses revealed that age-dependent endocytic pathology was accompanied by an increase in Rab GTPases in aged monkey brains. Here, we demonstrated that siRNA-induced dynein dysfunction reproduced the endocytic pathology accompanied by increased Rab GTPases seen in aged monkey brains and significantly disrupted exosome release. Moreover, it also resulted in endosomal β-amyloid precursor protein accumulation characterized by increased β-site cleavage. These findings suggest that dynein dysfunction may underlie age-dependent endocytic dysfunction via the up-regulation of Rab GTPases. In addition, this vicious circle may worsen endocytic dysfunction, ultimately leading to Alzheimer disease pathology.

The appearance of neuronal endocytic pathology before senile plaque deposition suggests that endocytic dysfunction is involved in early stage Alzheimer disease (AD)[2] pathology, such as the accumulation of β-amyloid precursor protein (APP) in enlarged early endosomes (1–4). β-Amyloid protein (Aβ), the major component of senile plaques, is produced from APP through sequential proteolytic cleavages by β- and γ-secretases, and such amyloidogenic cleavage, so-called β-site cleavage, of APP can occur through the endocytic pathway (1, 3). These findings suggest that endocytosis is involved in APP metabolism, and its dysfunction may lead to AD pathology. However, it remains unclear how endocytic dysfunction is induced in an age-dependent manner.

Cytoplasmic dynein is a microtubule-based motor protein required for minus end-directed axonal transport (5, 6). Dynactin, another microtubule-associated protein, binds to dynein intermediate chain (DIC) via its subunit, P150glued/dynactin (DYN) to form dynein-dynactin complexes that mediate minus end-directed vesicle transport, which includes endosome trafficking (7–12). We have previously shown that the interaction between DIC and DYN is clearly attenuated in aged monkey brains, suggesting that aging may impair dynein-mediated transport (13). Other studies also support this idea (14–17). Thus, in this study we investigated age-dependent endocytic pathology in cynomolgus monkey brains and tested our hypothesis of whether dysfunction of dynein causes endocytic dysfunction leading to AD pathology. Here, we demonstrated that siRNA-induced dysfunction of dynein reproduced the endocytic pathology and increased Rab GTPase levels observed in aged monkey brains. Moreover, dynein dysfunction also resulted in endosomal APP accumulation with a significant increase in β-site cleavage, representing early stage AD pathology.

EXPERIMENTAL PROCEDURES

Animals—Fourteen cynomolgus monkey (*Macaca fascicularis*) brains were used in this study. Of these, 6 brains were from young monkeys (ages 4 and 6 years), and 8 were from aged monkeys (ages 25, 26, 32, and 36 years). The frontal and temporal lobes of all the brains were used for immunohistochemical studies. The temporal lobes of eight cases (ages 4 years (n = 4), 25 years (n = 2), 26 years (n = 2)) were used for Western blot analyses.

All brains were obtained from the Tsukuba Primate Research Center, National Institute of Biomedical Innovation, Japan. All animals were housed in individual cages and maintained according to the National Institute of Biomedical Innovation

* This work was supported by a grant-in-aid from Comprehensive Research on Aging and Health, Ministry of Health, Labor, and Welfare, Japan.
[S] The on-line version of this article (available at http://www.jbc.org) contains a supplemental table and Figs. 1–3.
[1] To whom correspondence should be addressed. Fax: 81-29-837-0218; E-mail: kimura@nibio.go.jp.
[2] The abbreviations used are: AD, Alzheimer disease; APP, β-amyloid precursor protein; Aβ, β-amyloid protein; DIC, dynein intermediate chain; DYN, P150glued/dynactin; TGN, trans-Golgi network; TfR, transferrin receptor; DHC, dynein heavy chain; Flo-1, flotillin-1; sAPPα, secreted fragment of APP by α-secretase; sAPPβ, secreted fragment of APP by β-secretase; αCTF, C-terminal fragment of APP by α-secretase; βCTF, C-terminal fragment of APP by β-secretase; PBS, phosphate-buffered saline; siRNA, small interfering RNA; OA, okadaic acid.

rules and guidelines for experimental animal welfare. Three monkeys (ages 26 and 36 years) died naturally. The remaining animals were deeply anesthetized with pentobarbital.

Antibodies—In this study we used the following antibodies: mouse monoclonal anti-β-actin antibody (Sigma), mouse monoclonal anti-α-tubulin antibody (Santa Cruz Biotechnology, Santa Cruz, CA), mouse monoclonal anti-DIC antibody (Chemicon, Temecula, CA), mouse monoclonal anti-secreted fragment of APP by α-secretase (sAPPα) antibody (IBL, Gunma, Japan), mouse monoclonal anti-Aβ40 C-terminal 35–40 residue antibody (1A10; IBL), mouse monoclonal anti-rodent Aβ N-terminal antibody (14F1; IBL), mouse monoclonal anti-Rab5 antibody (Rab5m; Santa Cruz Biotechnology), mouse monoclonal anti-Rab11 antibody (Rab11m; Abcam, Cambridge, UK), mouse monoclonal anti-trans-Golgi network (TGN) antibody (Abcam), mouse monoclonal anti-Alix antibody (Santa Cruz Biotechnology), mouse monoclonal anti-transferrin receptor (TfR) antibody (Zymed Laboratories Inc., Carlsbad, CA), rabbit polyclonal anti-dynein heavy chain (DHC) antibody (Santa Cruz Biotechnology), rabbit polyclonal anti-DYN antibody (Santa Cruz Biotechnology), rabbit polyclonal anti-Rab5 antibody (Rab5r; Santa Cruz Biotechnology), rabbit polyclonal anti-Rab7 antibody (Rab7; Sigma), rabbit polyclonal anti-Rab11 antibody (Rab11r; Abcam), rabbit polyclonal anti-flotillin-1 (Flo-1) antibody (Santa Cruz Biotechnology), rabbit polyclonal anti-APP N-terminal antibody (APPn; IBL), rabbit polyclonal anti-APP C-terminal antibody (APPc; Zymed Laboratories Inc.), and rabbit polyclonal anti-secreted fragment of APP by β-secretase (sAPPβ) antibody (IBL). APPn predominantly recognizes full-length APP in Neuro2a cells (data not shown), and then it was used for immunocytochemistry. Because APPc can recognize both full-length APP and C-terminal fragment of APP by α-secretase (αCTF) or β-secretase (βCTF), it was used for Western blot analyses.

Immunohistochemistry—Immunostaining of monkey brains was performed as described elsewhere (18). Briefly, the brain samples were immersion-fixed with 4% paraformaldehyde, embedded in paraffin, and cut into 4-μm-thick sections. The sections were deparaffinized by pretreating with 0.5% periodic acid followed by autoclaving for 5 min at 121 °C, then incubated with a primary antibody solution overnight at 4 °C. In this study we used the following primary antibodies: anti-Rab5r (1:100), anti-Rab7 (1:200), and anti-Rab11r (1:200). After brief washes with buffer, the sections were sequentially incubated with biotinylated goat anti-mouse or anti-rabbit IgG then with a streptavidin-biotin-horseradish peroxidase complex (sABC kit; DAKO, Denmark). Immunoreactive elements were visualized by treating the sections with 3–3′ diaminobenzidine tetroxide (Dojin Kagaku, Japan). The sections were then counterstained with hematoxylin.

Subcellular Fractionation of Monkey Brains—Subcellular fractions from the temporal lobes of 8 monkeys were prepared at 0–4 °C as described by Tamai *et al.* (19). Briefly, sucrose solutions were prepared in a buffer containing 10 mM Tris-HCl (pH 7.6), 0.25 mM phenylmethylsulfonyl fluoride, and 1 mM EDTA. Brain tissue (~1.0 g) was homogenized in a glass homogenizer with 10 ml of 0.32 M sucrose solution and then centrifuged at 1000 × *g* for 10 min. The pellet (P1) was resuspended in 0.32 M sucrose, and this solution was layered over a discontinuous density gradient consisting of 1.2 and 0.85 M sucrose solutions. The suspension was centrifuged at 75,000 × *g* for 30 min in a Hitachi RPS-27 swing rotor to separate out P1 myelin and nuclei fractions. The supernatant (S1) from the P1 fraction was centrifuged at 13,000 × *g* for 15 min to yield the P2 fraction. The supernatant (S2) from the P2 fraction was centrifuged at 105000 × *g* for 60 min to obtain the microsomal (pellet) and cytosol (supernatant) fractions.

In this study we used the microsomal fraction for Western blot analyses. To normalize loading differences and confirm the purity of the fraction, we immunoblotted the fractions as described previously (20). Endoplasmic reticula and vesicles in the microsomal fraction were examined with mouse monoclonal anti-calnexin antibody (Santa Cruz Biotechnology; 1:500).

Western Blot Analyses for Age-related Changes in Rab GTPases in Monkey Brains—The proteins in the microsomal fractions were adjusted to 10 μg, and then each fraction was analyzed using SDS-PAGE and 12.5% acrylamide gels. Separated proteins were blotted onto polyvinylidene fluoride membranes (Immobilon P; Millipore, Bedford, MA). The membranes were blocked with 5% nonfat dried milk in 20 mM PBS (pH 7.0) and 0.1% Tween 20 for 1 h at room temperature and then incubated with primary antibodies overnight at 4 °C. In this study we used the following primary antibodies: anti-Rab5r (1:1000), anti-Rab7 (1:5000), and anti-Rab11r (1:5000). They were then incubated with either horseradish peroxidase-conjugated goat anti-mouse IgG or goat anti-rabbit IgG (Cell Signaling Technology, Danvers, MA) for 1 h at room temperature. Immunoreactive elements were visualized using enhanced chemiluminescence (Immobilon Western Detection Reagents; Millipore).

Cell Cultures—COS-7 cells were cultured in culture medium (Dulbecco's modified Eagle's medium with 10% fetal calf serum). Cells were plated at 2.0×10^4 cells/cm^2 onto 6-well plates coated with 0.01% poly-L-lysine (Wako, Osaka, Japan) for Western blot analyses and at 1.0×10^4 cells/cm^2 onto 2-well LAB-TEK chamber slides (Nalge Nunc, Rochester, NY) coated with 0.01% poly-L-lysine for immunocytochemistry. A neuronal cell line, mouse neuroblastoma Neuro2a cells, was also cultured in culture medium. Cells were plated at 1.5×10^4 cells/cm^2 onto 6-well plates coated with 0.01% poly-L-lysine for Western blot analyses at 1.5×10^4 cells/cm^2 onto 60-mm dishes coated with 0.01% poly-L-lysine for immunoprecipitation and at 1.0×10^4 cells/cm^2 onto 2-well LAB-TEK chamber slides (Nalge Nunc) coated with 0.01% poly-L-lysine for immunocytochemistry.

RNA Interference—For double-stranded RNA-mediated interference (RNAi) experiments we used the following short double-stranded RNA (siRNA) against primate-specific DHC (siDHC) and DYN (siDYN) for COS-7 cells and against mouse-specific DHC (siDHCm) for Neuro2a cells: siDHC, 5′-GGUGGGUGUACAUUACGAAUU-3′ (sense) and 5′-UUCGUAAUGUACACCCACCUG-3′ (antisense); siDYN, 5′-GGAGCGCUGUAUCGUAAGACC-3′ (sense) and 5′-UCUUACGAUACAGCGCUCCAG-3′ (antisense); siDHCm, 5′-GUAUCAGCACGGAGUUUUUGG-3′ (sense) and 5′-AAAAACUCCGUGC-

UGAUACUC-3′ (antisense). To avoid off-target effects, all siRNAs were carefully designed by Enhanced siDirect®. We also examined two different siRNAs for each target (see the supplemental table) and confirmed their knockdown-specific effects (data not shown). The control siRNA had a random sequence. RNAi experiments were performed by using siLentFect™ lipid reagent (Bio-Rad) according to the manufacturer's protocol.

Twenty-four or seventy-two hours after siRNA transfection, cells plated on 6-well plates were harvested in PBS and centrifuged to obtain cell pellets. The pellets were lysed in a sample buffer solution containing 62.5 mM Tris-HCl (pH 6.8), 2 mM EDTA, 0.5% Triton X-100, 2% SDS, and Complete Mini™ proteinase inhibitor mixture (Roche Applied Science) to extract total cellular proteins. Total proteins were adjusted to 10 μg and then subjected to SDS-PAGE by using 6% (DHC), 12.5% (other proteins), or 16% acrylamide gels (αCTF, βCTF, and Aβ). Separated proteins were blotted onto nitrocellulose membranes (Pall Life Sciences, Ann Arbor, MI) (Aβ) or polyvinylidene fluoride membranes (other proteins). Blotted nitrocellulose membranes were heated in boiling PBS for 5 min to enhance the signal (21) and then subjected to Western blot analyses as described above. We used the following primary antibodies: anti-β-actin (1:50000), anti-DHC (1:500), anti-DIC (1:20000), anti-DYN (1:2000), anti-Rab5r, anti-Rab7, anti-Rab11r, anti-APPc (1:1000), anti-sAPPα (1:1000), anti-sAPPβ (1:5000), and anti-Aβ40 C-terminal (1:500). We performed three independent experiments ($n = 6$ for each experimental group), duplicating each experiment.

Cells plated on chamber slides were fixed with 4% paraformaldehyde and then permeabilized with 0.01% (COS-7) or 0.1% (Neuro2a) Triton X-100 for 5 min at room temperature. After blocking with 3% bovine serum albumin, cells were incubated with primary antibodies overnight at 4 °C. Cells were then incubated with AlexaFluor 488-conjugated anti-mouse IgG and AlexaFluor 555-conjugated anti-rabbit IgG (Invitrogen) for 1 h at room temperature. All cells were examined with a Digital Eclipse C1 confocal microscope (NIKON, Kanagawa, Japan). For immunocytochemistry, we used the following primary antibodies: anti-DIC (1:10000), anti-Rab5m (1:1000), anti-Rab11m (1:200), anti-TGN (1:1000), anti-DYN (1:1000), anti-Rab5r (1:5000), anti-Rab7r (1:10000), anti-Rab11r (1:10000), and anti-APPn (1:2000). We performed three independent experiments.

Drug Treatments—COS-7 cells were treated with the following drugs at the indicated final concentrations: chloroquine (5 and 10 μM) and NH_4Cl (5 and 10 mM), both purchased from Wako. Neuro2a cells were cultured in serum-free culture medium containing 1% insulin-transferrin-selenium X supplement (Invitrogen) and then treated with okadaic acid (OA; 1 and 5 nM) (Calbiochem) dissolved in DMSO for 24 or 48 h. To wash and harvest cells treated with OA, we used PBS containing 10 mM NaF (Wako) and 2 mM Na_3VO_4 (Wako) to avoid dephosphorylation. Western blot analyses and immunocytochemistry were performed as described above. For Western blot analyses, we used the following primary antibodies: anti-β-actin, anti-DIC, anti-DYN, anti-Rab5r, anti-Rab7, and anti-Rab11r. We performed three independent experiments ($n = 6$ for each experimental group), duplicating each experiment. For immunocytochemistry, we used the following primary antibodies: anti-DIC, anti-α-tubulin (1:1000), anti-DYN, anti-Rab5r, anti-Rab7, and anti-Rab11r. We performed three independent experiments.

Semiquantitative Reverse Transcription-PCR—Primer sets were designed to recognize and amplify nucleotide sequences encoding mouse DHC (NM_030238), APP (NM_007471), and β-actin (NM_007393). cDNA sequences and/or the homologue(s) was identified using the BLAST (Basic Local Alignment Search Tool) computer program (National Center for Biotechnology Information, Bethesda, MD). Primers were designed using the Primer3 computer program (Whitehead Institute, Cambridge, MA).

Seventy-two hours after siRNA transfection, total cellular RNAs from Neuro2A cells were isolated using TRIzol reagent (Invitrogen). Single-stranded cDNAs were prepared via reverse transcription of a reaction mixture of total RNA (1 μg in 20 μl of reaction mixture), oligo$(dT)_{12-18}$ primers, and Superscript™II (Invitrogen). PCR amplification was performed using Thermo-Start™ (Thermo Fisher Scientific, Epsom, UK) and the following primers: DHC (+), 5′-CTCGGAAGCTTCGACAAAAC-3′; DHC (−), 5′-TCATCAGCTGTTTCCAGTGC-3′; APP (+), 5′-GGTTCTGGGCTGACAAACAT-3′; APP (−); 5′-GTGATGACAATCACGGTTGC-3′ β-actin (+); 5′-ATGGATGACGATATCGCTG-3′; β-actin (−), 5′-ATGAGGTAGTCTGTCAGGT-3′.

PCR products were electrophoresed in 1.5% agarose gels, and gels were subsequently stained with ethidium bromide. Densitometric analyses of gels were carried out with Quantity One Software (PDI Inc.). We performed three independent experiments ($n = 6$ for each experimental group), duplicating each experiment.

Immunoprecipitation—All steps were performed at 4 °C unless otherwise noted. For immunoprecipitation, we used recprotein G-Sepharose® 4B beads (Zymed Laboratories Inc.). Seventy-two hours after siRNA treatment, Neuro2a cell cultures (60 mm dish) were lysed in immunoprecipitation buffer solution containing 25 mM Tris-HCl (pH 8.0), 0.5% Triton X-100, 0.5% Nonidet P-40, and Complete Mini™ proteinase inhibitor mixture and then centrifuged at 105,000 × *g* for 15 min. The supernatant was recovered and then precleaned with Sepharose beads for 1 h. The precleaned supernatant containing 10 μg of proteins was incubated with anti-Aβ40 C-terminal antibody (1A10; 1 μg) or mouse IgG (Rockland Immunochemicals, Gilbertsville, PA) for 2 h. After immunoreactions, antibody-linked supernatant was incubated with precleaned beads for 1 h. The beads were washed with lysis buffer twice and then finally with Tris-buffered saline (50 mM Tris-HCl, pH 6.8). Protein was eluted from the beads with electrophoresis sample buffer and then analyzed using SDS-PAGE (16% acrylamide gels). Separated proteins were blotted onto nitrocellulose membranes. Blotted nitrocellulose membranes were heated in boiling PBS for 5 min to enhance the signal (21) and then subjected to Western blot analyses with anti-rodent Aβ N-terminal antibody (14F1; 1:2000). We performed five independent experiments.

Preparation of the Extracellular Membrane Fraction—Seventy-two hours after siRNA treatment, culture media from

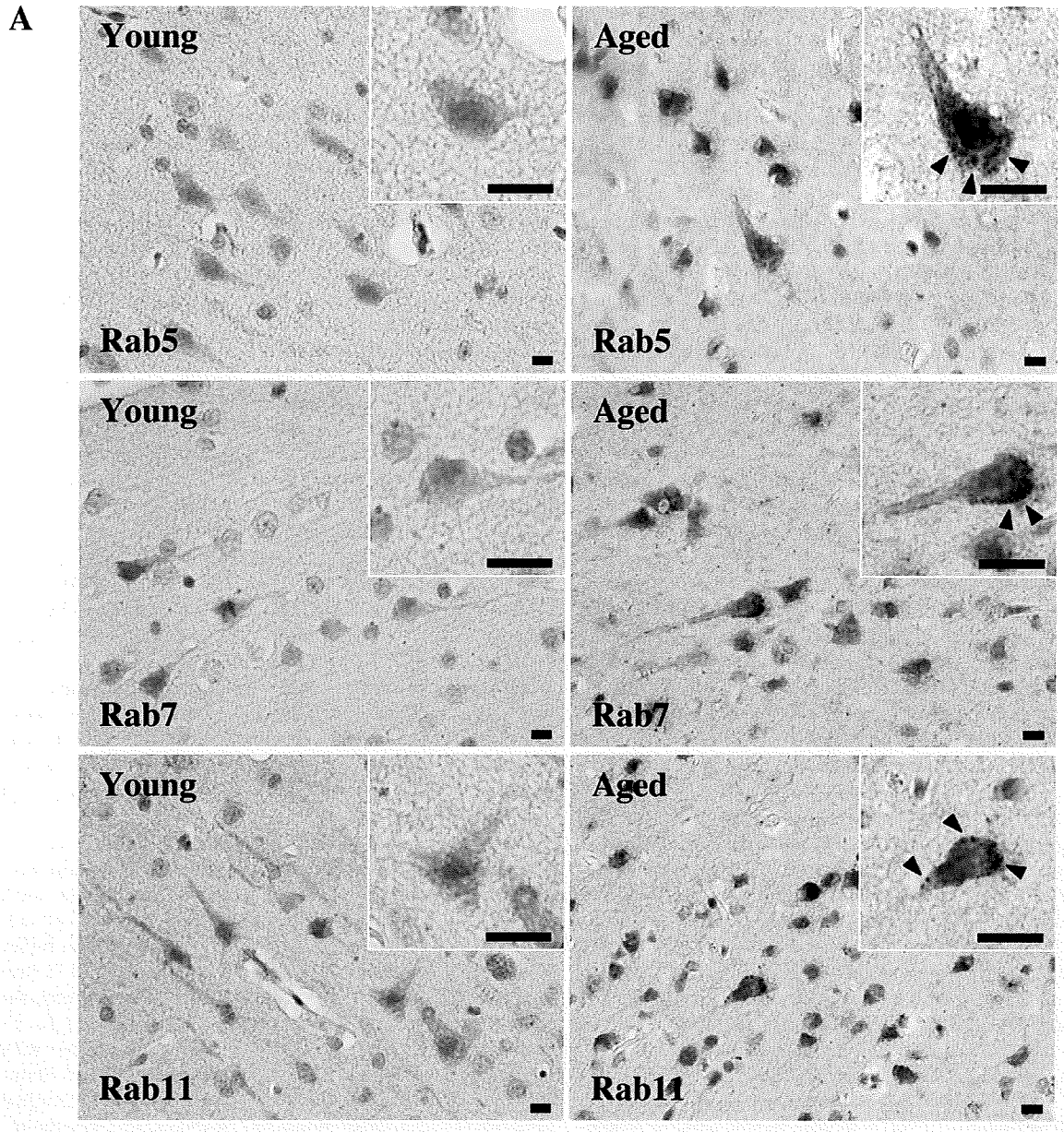

each well of Neuro2a cell cultures (6-well plate) were collected and centrifuged for 10 min at 1000 × *g* to exclude cell debris. The supernatant was subjected to ultracentrifugation at 10,000 × *g* for 30 min and at 100,000 × *g* for 1 h. The resulting pellets were resuspended in sample buffer and then subjected to Western blot analyses. We used the following primary antibodies: anti-Alix (1:1000), anti-Flo-1 (1:10000), anti-TfR (1:10000), and anti-APPc. We examined 12 independent samples for each group.

Data Analyses—To confirm reproducibility, immunoreactive bands obtained from the Western blots were quantified using commercially available software (Quantity One; PDI, Inc., Upper Saddle River, NJ). Data are shown as the means ± S.D. For statistical analyses, one-way analysis of variance was performed followed by the Bonferroni Dunn post hoc test.

RESULTS

Age-dependent Endocytic Pathology Is Observed in Aged Monkey Brains, and Rab GTPases Are Concurrently Increased—The cynomolgus monkey is a good animal model for studying age-dependent Aβ pathology without transgenic manipulations (18, 22, 23). Thus, we used this model first to investigate whether aging itself causes endocytic pathology in monkey brains. Immunohistochemical analyses revealed that early (Rab5-positive), late (Rab7-positive), and recycling (Rab11-positive) endosomes were apparently enlarged mainly in large pyramidal neurons of aged monkey brains (Fig. 1*A*). Endosome trafficking is regulated by small Rab GTPases such as Rab5, Rab7, and Rab11 (24). Therefore, to investigate the relationship between age-dependent endocytic pathology and Rab GTPase levels, we performed Western blot analyses on tissue from the same monkey brains used for immunohistochemistry. In aged monkey brains, the amounts of Rab GTPases were significantly increased respectively (Fig. 1, *B* and *C*).

siRNA-induced Dysfunction of Dynein Causes Endocytic Pathology with a Concomitant Increase in Rab GTPases—We previously showed that dynein-dynactin interactions are attenuated in aged monkey brains, suggesting that dynein-mediated transport in aged brains is dysfunctional (13). To test our hypothesis that dysfunction of dynein-mediated transport may cause the age-dependent endocytic pathology observed in aged monkey brains, we performed RNAi experiments using COS-7 cells. COS-7 cells have large somas and are, thus, useful for studying endosomal trafficking. We chose DHC as a main target to knock down because it is well known that siRNAs targeting DHC also induce significant down-regulation of DIC (25). DHC has an ATPase activity for dynein-mediated transport, and DIC interacts with DYN to assemble dynein-dynactin complexes responsible for minus end-directed vesicle transport (5–12, 26). Hence, the depletion of both DHC and DIC should cause severe dysfunction of dynein-mediated transport.

In siDHC-transfected cells, both DHC and DIC expression levels clearly dropped 24 h after transfection, indicating effective depletion of dynein (Fig. 2*A*). Dynein depletion noticeably lasted up to 72 h after transfection (Fig. 2*A*). In contrast to control siRNA-transfected cells, in siDHC-transfected cells dynein depletion resulted in an increase in Rab7 24 h after transfection; this increase became significant 72 h after transfection (Fig. 2, *A* and *B*). Unlike Rab7, Rab5 expression levels remained more or less the same 24 h after transfection before increasing at the 72-h point (Fig. 2, *A* and *B*). Interestingly, Rab11 expression clearly increased 24 h after transfection, but it increased even more 72 h after transfection (Fig. 2, *A* and *B*). Dynein depletion also resulted in a significant increase in DYN (Fig. 2, *A* and *B*).

To confirm the relationship between elevated Rab GTPase levels and endocytic pathology, we immunostained cells with antibodies against various Rab GTPases 72 h after siRNA transfection. DIC-negative cells (*i.e.* cells depleted of dynein) possessed enlarged endosomes that showed variable localization patterns (Fig. 2*C*). By contrast, Rab7-positive endosomes mainly localized around nuclei in control siRNA-transfected cells and enlarged Rab7-positive endosomes distributed around nuclei as well as in peripheral parts of the cytoplasm (Fig. 2*C*). The localization of Rab11-positive endosomes showed the most drastic change. In control siRNA-transfected cells, most Rab11-positive endosomes gathered and localized to the juxtanuclear region, also known as the juxtanuclear endocytic recycling compartment (Fig. 2*C*). The depletion of dynein disrupted the juxtanuclear assembly of Rab11-postive endosomes such that enlarged Rab11-positive endosomes distributed throughout the cytoplasm (Fig. 2*C*). Although Rab5 expression only increased slightly, even 72 h after transfection both Rab7 and Rab11 expression increased significantly due to the depletion of DYN (supplemental Fig. S1). Interestingly, the depletion of DYN resulted in the significant increase in DIC (supplemental Fig. S1).

Drug-induced Perturbation of Endosome Trafficking to Lysosomes Can Also Cause Recycling Endocytic Pathology—Recruitment of recycling endosomes to endocytic recycling compartment is mediated by dynein (27, 28). To assess whether recycling endocytic pathology is directly caused by disturbance of its recruitment or whether it represents a secondary consequence of disrupting endosome trafficking to the lysosomal degradation pathway, we examined how chloroquine and ammonium chloride, two drugs well known to perturb endosome trafficking to lysosomes independent of dynein function (29), affect the levels of endosome-related GTPases.

FIGURE 1. **Endocytic pathology accompanied by increase in Rab GTPases in aged monkey brains.** *A*, photomicrographs of temporal lobe sections from a 4-year-old (*Young*) monkey and a 26-year-old (*Aged*) cynomolgus monkey are shown. Sections were immunostained with anti-Rab5r, anti-Rab7, and anti-Rab11r antibodies and then counterstained with hematoxylin. In aged monkey brains, early (Rab5-positive), late (Rab7-positive), and recycling (Rab11-positive) endosomes were enlarged mainly in large pyramidal neurons. The high magnification image (*inset*) shows enlarged endosomes (*arrowheads*) accumulated in an aged monkey brain. *Scale bars*, 10 μm. *B*, Western blots show the amounts of Rab5, Rab7, Rab11, and calnexin in microsomal fractions derived from 4- and 26-year-old monkey brains. The amounts of Rab GTPases were clearly increased in aged monkey brains. *C*, histograms show age-related changes in the amounts of Rab GTPases in young ($n = 4$) and aged ($n = 4$) monkey brains. All data were normalized according to calnexin levels. Values are the means ± S.D. *, $p < 0.01$; **, $p < 0.001$. *y* axes show the mean values of the quantified data.

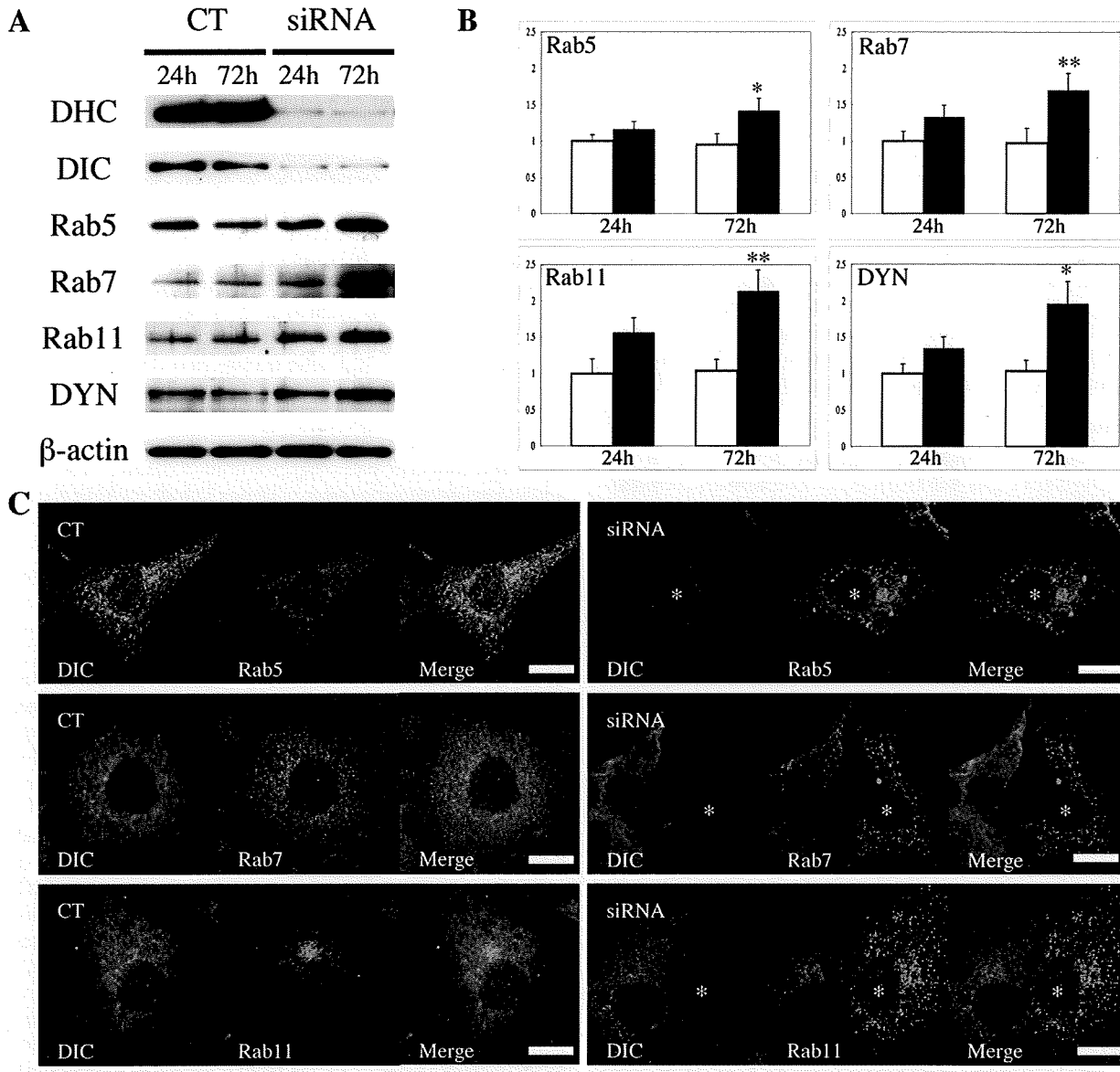

FIGURE 2. **siRNA-induced dynein dysfunction reproduces endocytic pathology accompanied by an increase in Rab GTPases.** *A*, Western blots show the amounts of DHC, DIC, Rab5, Rab7, Rab11, DYN, and β-actin in extracts derived from COS-7 cells 24 and 72 h after siRNA transfection. The amounts of DHC and DIC clearly dropped even as soon as 24 h after transfection. The knockdown effectively lasted up to 72 h after transfection. The depletion of dynein resulted in the time-dependent increase in Rab GTPases and DYN in COS-7 cells. *B*, histograms show the effect of dynein depletion on the amounts of Rab GTPases and DYN in COS-7 cells. The increase in Rab7 preceded that of Rab5 and became significant 72 h after transfection. The amount of Rab11 began to increase as early as 24 h after transfection and became quite significant 72 h after transfection. The amount of DYN also significantly increased 72 h after transfection. All data were normalized according to β-actin levels. Values are the means ± S.D. $*p < 0.05$; $**p < 0.001$. *y* axes show the mean values of the quantified data. *C*, photomicrographs of COS-7 cells immunostained for DIC, Rab5, Rab7, and Rab11 72 h after siRNA transfection. The depletion of dynein resulted in the accumulation of enlarged endosomes. *Scale bars*, 10 μm. *CT*, cells transfected with control si-RNA; *siRNA*, cells transfected with siDHC. *Asterisks*, DIC-immunonegative cells (dynein-depleted cells).

As expected, both chloroquine and ammonium chloride significantly increased Rab5 and Rab7 expression, respectively. Moreover, enlarged Rab5- and Rab7-positive endosomes were clearly observed in treated cells, indicating that endocytic dysfunction was successfully induced (Fig. 3). Noteworthy, Rab11 significantly increased after the drug treatments, and enlarged Rab11-positive endosomes were also observed (Fig. 3).

siRNA-induced Dysfunction of Dynein Results in Endosomal APP Accumulation Leading to Enhancement of β-Site Cleavage and Also Disturbs Exosome Release—Finally, to test our hypothesis that dysfunction of dynein may cause endocytic dysfunction leading to early-stage AD pathology, we performed RNAi experiments using a neuronal cell line, Neuro2a. As with COS-7 cells, Neuro2a cells depleted of

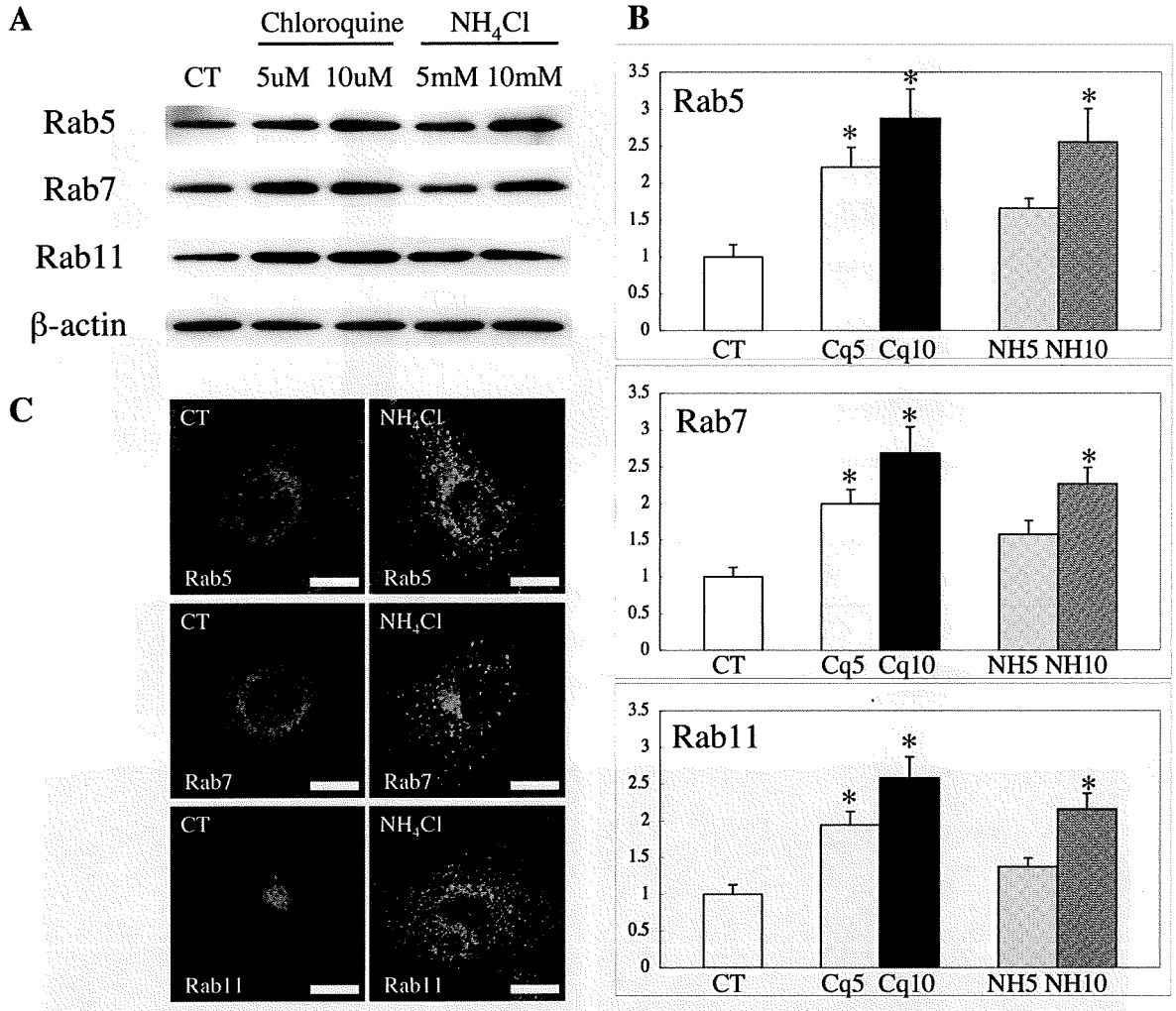

FIGURE 3. **Drug treatment reproduced recycling endocytic pathology independent of dynein function.** *A*, Western blots show the amounts of Rab5, Rab7, Rab11, and β-actin in COS-7 cells treated with chloroquine and ammonium chloride (NH_4Cl). Drug treatments induced increases in Rab GTPases levels but not β-actin levels, which remained unchanged. *B*, histograms show the effect of drug treatments on Rab GTPases levels. All data were normalized according to β-actin levels (*CT*, control). Values are the means ± S.D. *, $p < 0.05$. *C*, photomicrographs of COS-7 cells immunostained for Rab5, Rab7, and Rab11 24 h after drug treatment. NH_4Cl treatment induced enlargement not only of early (Rab5-positive) and late (Rab7-positive) endosomes but also of recycling endosomes (Rab11-positive). *Scale bars*, 10 μm. *Cq*, cells treated with chloroquine; *NH*, cells treated with NH_4Cl. *y* axes show the mean values of the quantified data.

dynein also showed a significant increase in Rab GTPases (supplemental Fig. S2). Because dynein-dynactin complexes associate with vesicle cargo via dynactin (30–35), DYN can be used as a marker for minus end-directed vesicle cargo. Immunocytochemical analyses demonstrated that DYN accumulated in the distal ends of neurite-like processes due to depletion of dynein (supplemental Fig. S2), indicating that dynein depletion disturbed minus end-directed vesicle transport.

In this study we aimed to examine endogenous APP metabolism. Noteworthy, dynein depletion significantly increased endogenous APP and its β-site cleavage products such as sAPPβ, βCTF, and Aβ, respectively (Fig. 4, *A* and *B*). Immunoprecipitation analyses also confirmed that the amount of Aβ was increased in siDHCm-transfected cells (Fig. 4*C*). APP can be alternately cleaved by α-secretase within the Aβ domain, resulting in productions of sAPPα and αCTF (36, 37). In contrast to β-site cleavage products, the amount of sAPPα and αCTF seemed unchanged by dynein depletion (Fig. 4, *A* and *B*). Immunocytochemical analyses confirmed that APP clearly accumulated in dynein-depleted cells and mainly localized to enlarged Rab5-positive endosomes, *i.e.* early endosomes (Fig. 4*F*). Moreover, dynein depletion also caused APP to accumulate in the distal ends of neurite-like processes (Fig. 4*F*).

To determine whether exosome secretion pathway is also affected by dynein dysfunction, we prepared extracellular membrane fractions from siRNA-transfected Neuro2a cells 72 h after transfection. In contrast to control siRNA-transfected cells, the amounts of both Alix and Flo-1, two exosome markers, were significantly decreased in extracellular membrane fractions derived from dynein-depleted cells (Fig. 4*G*).

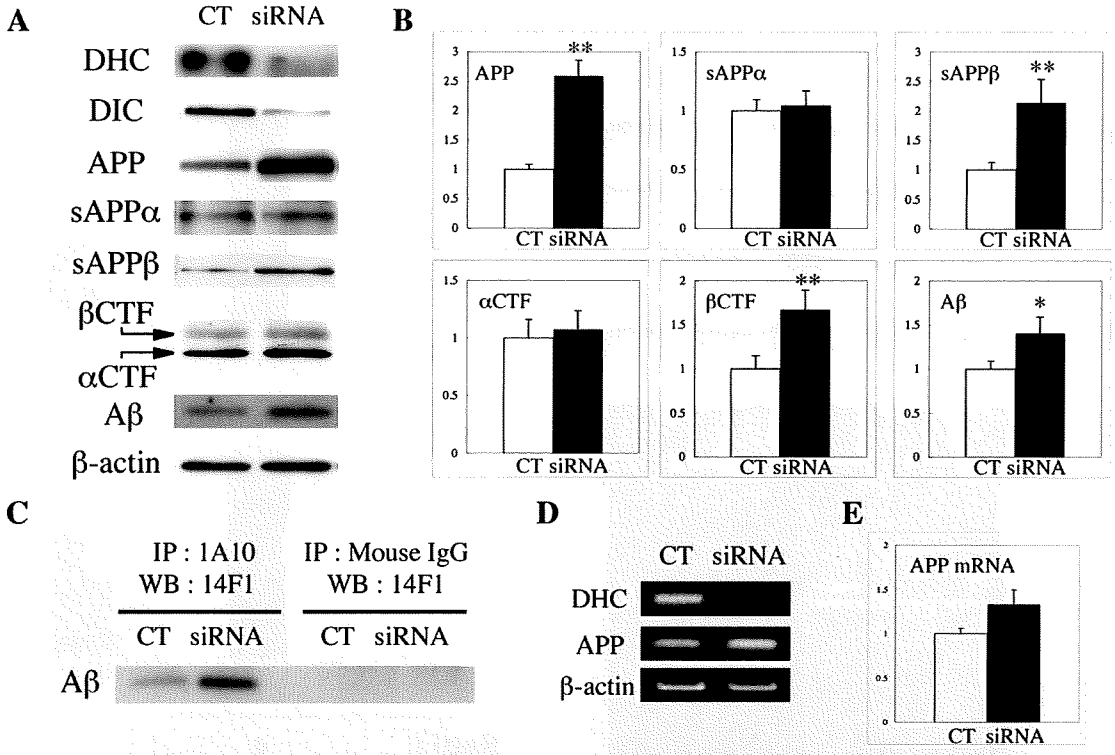

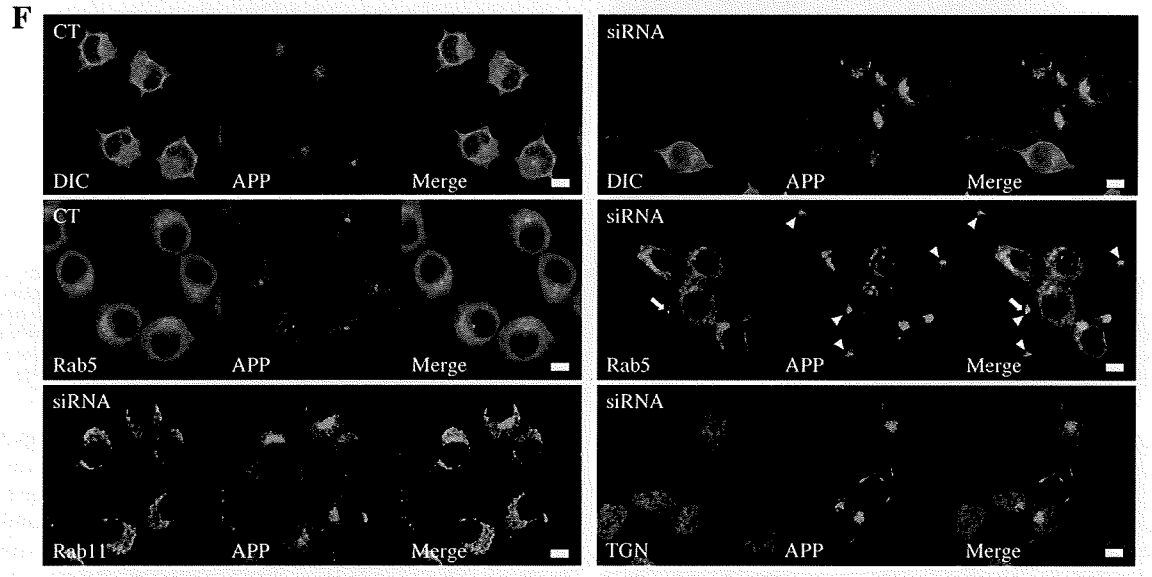

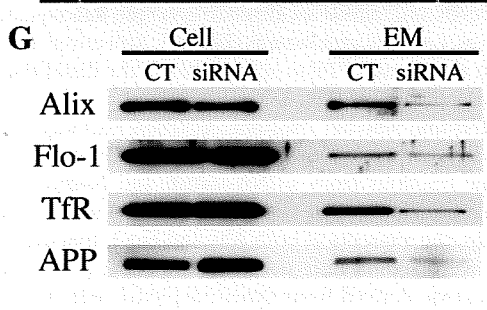

Furthermore, TfR and APP levels were also considerably decreased in extracellular membrane fractions (Fig. 4*G*).

DISCUSSION

Here, we demonstrated that dysfunction of dynein causes multi-endocytic pathology with an increase of Rab GTPases, and it may underlie age-dependent endocytic dysfunction leading to early stage of AD pathology such as endosomal accumulation of APP.

In this study immunohistochemical analyses of monkey brains indicated that age-dependent endocytic pathology was accompanied by an increase in Rab GTPases (Fig. 1). A recent study showed that over-activation of Rab GTPase causes aberrant up-regulation of endosome trafficking and endocytosis, resulting in endocytic pathology (38). Taken together, these findings suggest that aging can cause an increase in Rab GTPases and induce endocytic pathology.

We previously showed that dynein-dynactin interactions are attenuated in aged monkey brains (13). Because the dynein-dynactin complex mediates endosome trafficking (39–43), we hypothesized that age-dependent dysfunction of dynein-mediated transport disrupts endosome trafficking, resulting in the compensatory up-regulation of Rab GTPases. Our RNAi experiments demonstrated that the depletion of dynein induced a significant increase in Rab GTPases. Immunocytochemical analyses confirmed endocytic pathology in the dynein-depleted cells (Fig. 2). This finding suggests that dynein dysfunction itself can cause aberrant up-regulation of endosome trafficking, leading to endocytic pathology. Importantly, the aberrant up-regulation of endosome trafficking also perturbs dynein-mediated transport (38). Thus, the dysfunction of dynein and the up-regulation of endosome trafficking may represent a "vicious circle" that leads to endocytic dysfunction.

In the present study the increase of Rab7 preceded that of Rab5 (Fig. 2), suggesting that dynein dysfunction primarily or strongly affects the trafficking of late endosomes before subsequently affecting the trafficking of early endosomes retrogradely. Because dynein mediates the fusion of late endosomes with lysosomes (39, 41, 43, 44), dynein dysfunction would perturb fusion, resulting in impairment of lysosomal degradation (Fig. 5). Thus, it is reasonable that the compensatory up-regulation of Rab7 would primarily be necessary to ensure cell viability, as Rab7 up-regulation enhances trafficking of late endosomes to fuse with lysosomes. Indeed, dynein dysfunction also resulted in an increase in Rab11, the recycling endosome-associated Rab GTPase (Fig. 2). Our drug treatment experiments confirmed that drug-induced perturbation of endosome trafficking to lysosomes increases Rab11 and causes recycling endocytic pathology (Fig. 3). Hence, although we cannot fully exclude the possibility that dynein dysfunction directly disturbs the recruitment of recycling endosomes to endocytic recycling compartment, impaired trafficking of late endosomes to lysosomes may shift early endosomes to the recycling pathway to avoid intracellular vesicle accumulations.

Intriguingly, the depletion of dynein caused a significant increase in DYN, whereas the depletion of DYN caused a significant increase in DIC and vice versa (Fig. 1, supplemental Fig. S1). This finding suggests that dysfunction of one component of the dynein-dynactin complex may induce compensatory up-regulation of the other component. Because we have previously shown that DYN levels were significantly increased in aged monkey brains (13), age-dependent dysfunction of minus end-directed vesicle transport may be caused by a dysfunction in dynein rather than dynactin.

Most noteworthy, our RNAi experiments with Neuro2a cells demonstrated that dysfunction of dynein caused intracellular accumulation of APP, which was accompanied by a significant increase in β-site cleavage products, resulting in intracellular accumulation of Aβ (Fig. 4). Because neither sAPPα nor αCTF showed significant changes in dynein-depleted cells, dynein dysfunction would not affect α-site cleavage. Immunocytochemistry also confirmed early-stage AD pathology, such as APP accumulation in enlarged early endosomes. Although semiquantitative reverse transcription-PCR analyses showed that the APP mRNA level seemed rather increased in dynein-depleted cells, APP mainly accumulates in enlarged early endosomes but not recycling endosome or TGN, and the APP level in extracellular membrane fraction was significantly decreased (Fig. 4). These findings suggest that APP endocytosis is really induced by the dysfunction of dynein, and intracellular accumulation of APP would not be the simple consequence of enhanced APP expression but may be attributed to endosomal retention and subsequent avoidance of lysosomal degradation. Although additional studies are needed, this finding suggests that dysfunction of dynein-mediated transport is involved at least partly in age-dependent AD pathology via endocytic dysfunction. Moreover, the dysfunction of dynein also

FIGURE 4. **siRNA-induced dysfunction of dynein caused endosomal APP accumulation with enhanced β-site cleavage and perturbed recycling endosome trafficking and exosome release in Neuro2a neuronal cells.** *A*, Western blots show the amounts of DHC, DIC, APP, sAPPα, sAPPβ, αCTF, βCTF, Aβ, and β-actin in extracts from Neuro2a cells 72 h after siRNA transfection. The amount of APP was clearly increased, and the amount of β-site cleavage products such as sAPPβ, βCTF, and Aβ also increased concurrently. *B*, histograms show the effect of dynein depletion on the amounts of APP, sAPPα, sAPPβ, αCTF, βCTF, and Aβ in Neuro2a cells. The depletion of dynein significantly increased APP, sAPPβ, βCTF, and Aβ 72 h after siRNA transfection. All data were normalized according to β-actin levels. Values are the means ± S.D. *, $p < 0.05$; **, $p < 0.001$. *y* axes show the mean values of the quantified data. *C*, shown are immunoprecipitation (*IP*) analyses of endogenous Aβ in Neuro2a cells 72 h after siRNA transfection. The amount of Aβ was clearly increased in siDHCm-transfected cells. *WB*, Western blot. *D*, expression patterns of DHC, APP, and β-actin mRNA in Neuro2a cells 72 h after siRNA transfection. Expression was assessed with semiquantitative reverse transcription-PCR. The expression of DHC mRNA clearly dropped in siDHCm-transfected cells, indicating successful siRNA-induced down-regulation of DHC. *E*, the histogram shows the effect of dynein depletion on the expression of APP mRNA in Neuro2a cells. Data were normalized according to β-actin levels. Values are the means ± S.D. *y* axes show the mean values of the quantified data. *F*, photomicrographs are shown of Neuro2a cells immunostained for DIC, Rab5, Rab11, TGN, and APP 72 h after siRNA transfection. The depletion of dynein resulted in the accumulation of APP, which mainly localized to enlarged early endosomes. *Scale bars*, 10 μm. *Arrows*, enlarged early endosomes in the distal ends of neurite-like processes; *arrowheads*, accumulations of APP in the distal ends of neurite-like processes. *G*, Western blots showing the amounts of Alix, Flo-1, TfR, and APP in whole-cell extracts and extracellular membrane (*EM*) fractions from Neuro2a cells 72 h after siRNA transfection. Dynein depletion significantly decreased the levels of Alix and Flo-1, two exosome markers, in extracellular membrane fractions but not in whole-cell extracts (*Cell*). The depletion of dynein also significantly decreased TfR and APP levels in EM 72 h after siRNA transfection. *CT*, cells transfected with control siRNA; *siRNA*, cells transfected with siDHCm.

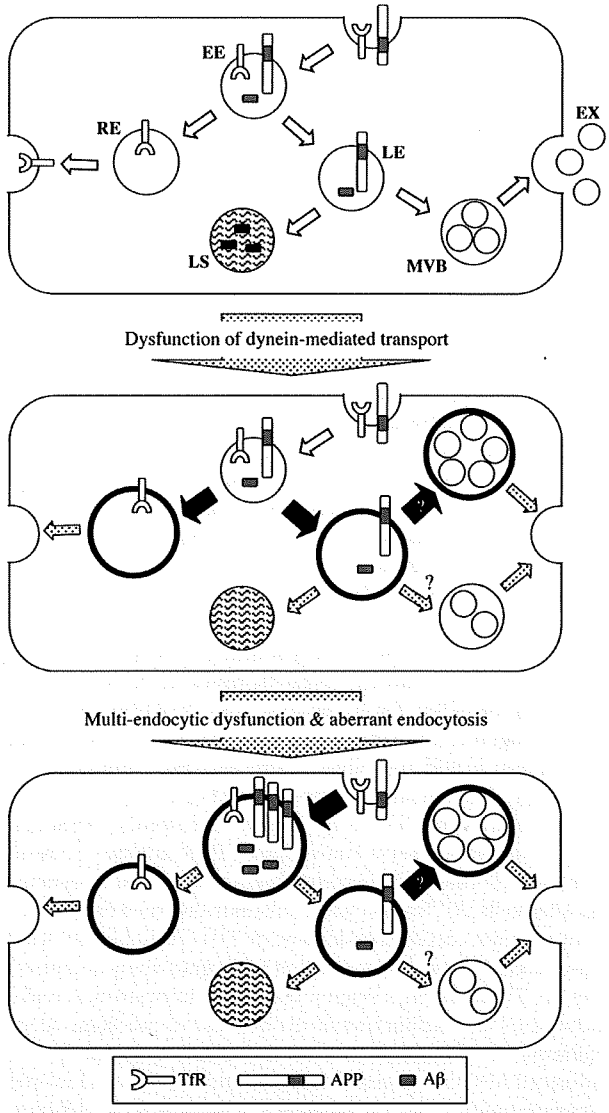

FIGURE 5. **Hypothetical scenario illustrating age-dependent endocytic dysfunction; a vicious circle leading to AD pathology.** We hypothesize that age-dependent dysfunction of dynein-mediated transport may cause compensatory up-regulation of Rab GTPase, resulting in up-regulation of endosome trafficking (*black solid arrows*). Consequently, the up-regulation of Rab GTPases causes endosomes to enlarge (*thick circle*), which in turn perturbs endosome trafficking (*dotted arrows*) and leads to the deterioration of dynein-mediated transport. This vicious circle may cause the unwanted uptake and/or accumulation of APP in early endosomes, and the retardation of endosome trafficking may result in enhanced endosomal β-site cleavage. Moreover, the disruption of recycling endosome trafficking and the decrease of exosome release may also cause intracellular protein/vesicle accumulation. Additional investigations are needed, however, to clarify whether multivesicular body (*MVB*) formation is up-regulated or down-regulated. *EE*, early endosome; *LE*, late endosome; *RE*, recycling endosome; *LS*, lysosome; *EX*, exosome.

caused APP accumulation in the distal ends of neurite-like processes (Fig. 4).

We previously showed that APP significantly accumulates in the nerve-ending fraction, which includes synaptic vesicles and membranes, from aged monkey brains (22). Intracellular Aβ content is also significantly increased in the nerve-ending fraction with aging (18). Our immunocytochemistry analyses revealed that APP accumulated within the distal ends of processes partly localized to Rab5-positive endosomes (Fig. 4). This suggests that age-dependent synaptic accumulation of APP may be caused not solely by age-dependent dysfunction of minus-end transport but also by local up-regulation of APP endocytosis. This, in turn, may lead to the concurrent accumulation of synaptic Aβ with the age-dependent down-regulation of neprilysin, an Aβ-degrading enzyme that mainly localizes to synapses (45).

We also demonstrated that dynein dysfunction significantly decreased exosome release (Fig. 4). Recent findings suggest that β-site cleavage may occur in multivesicular bodies (46) and that Aβ-containing exosomes are released into the extracellular space (47, 48). Although it remains unclear whether the release of Aβ represents a method of eliminating intracellular Aβ or simply achieves some other biological function, dynein dysfunction clearly decreased exosome release (Fig. 4) and may also lead to the accumulation of intracellular Aβ.

TfR levels in extracellular membrane fractions were also significantly decreased by the dysfunction of dynein even though TfR levels in whole-cell lysates did not significantly change (Fig. 4). This finding supports the premise that dynein dysfunction definitely disturbs recycling endosome trafficking. These findings suggest that dynein dysfunction may cause proteins to accumulate intracellularly by disturbing endosome trafficking at multiple levels, such as perturbations in lysosomal degradation, recycling endosome trafficking, and exosome release (Fig. 5). The intracellular accumulation of causative proteins is a common pathological feature of age-dependent neurodegenerative diseases (49–51). Although additional studies are needed, we propose that the age-dependent dysfunction of dynein may be a risk factor not only for AD but also for other age-dependent neurodegenerative diseases.

How aging causes dynein dysfunction remains unclear. One possible way is through the abnormal up-regulation of protein phosphorylation. Phosphorylation of DHC down-regulates DHC activity as an ATPase for transport (52, 53). On the other hand, phosphorylation of DIC causes it to detach from DYN, resulting in the dissociation of the dynein-dynactin complex (53). Several studies have shown that aging affects the activity of protein phosphatases in the brain (54–56) and that the activity of certain protein phosphatases, such as PP2A, is clearly decreased in AD brains (57–61). Moreover, neurofibrillary tangles, a late-stage neuropathological hallmark of AD, evidently result from the hyperphosphorylation of Tau protein (62). To assess the hypothesis that abnormal phosphorylation is responsible for age-related dynein dysfunction, we treated Neuro2a cells with the phosphatase inhibitor OA. Even at very low concentrations, OA treatment increased Rab7 levels in a dose- and time-dependent manner (supplemental Fig. S3). One study showed that OA treatment induces calpain activity leading to DIC degradation (63); however, we did not find evidence to support this observation at the dose used in the present study. Instead, OA treatment increased DYN levels, which is indicative of dynein dysfunction (supplemental Fig. S3). Immunocytochemistry confirmed that in OA-treated cells Rab7-positive

endosomes were enlarged, and their localization was affected even though microtubule assembly was not significantly changed (supplemental Fig. S3). These findings suggest that the increase in Rab7, reflecting dynein dysfunction, induced by OA treatment resulted neither from DIC depletion nor microtubule disruption. Because the colocalization of DIC and DYN was not appreciably affected by OA treatment at the dose we used (supplemental Fig. S3), dynein dysfunction may be caused by phosphorylation of DHC.

In conclusion, we demonstrated that dysfunction of dynein induces endocytic pathology accompanied by an increase in Rab GTPases, which may underlie age-dependent endocytic dysfunction. Although additional investigations are needed, we believe that this vicious circle continues to worsen endocytic dysfunction, ultimately leading to AD pathology such as the accumulation of intracellular APP and Aβ (Fig. 5). Moreover, because dynein also mediates the transport and fusion of autophagosomes with lysosomes (64–66), the intracellular transport system may represent a prime target for the development of new therapeutics used to treat not only AD but also other neurodegenerative disorders characterized by the abnormal intracellular accumulation of causative proteins.

REFERENCES

1. Cataldo, A. M., Barnett, J. L., Pieroni, C., and Nixon, R. A. (1997) *J. Neurosci.* **17,** 6142–6151
2. Cataldo, A. M., Peterhoff, C. M., Troncoso, J. C., Gomez-Isla, T., Hyman, B. T., and Nixon, R. A. (2000) *Am. J. Pathol.* **157,** 277–286
3. Cataldo, A. M., Petanceska, S., Terio, N. B., Peterhoff, C. M., Durham, R., Mercken, M., Mehta, P. D., Buxbaum, J., Haroutunian, V., and Nixon, R. A. (2004) *Neurobiol. Aging* **25,** 1263–1272
4. Nixon, R. A. (2005) *Neurobiol. Aging* **26,** 373–382
5. Lye, R. J., Porter, M. E., Scholey, J. M., and McIntosh, J. R. (1987) *Cell* **51,** 309–318
6. Paschal, B. M., Shpetner, H. S., and Vallee, R. B. (1987) *J. Cell Biol.* **105,** 1273–1282
7. Gill, S. R., Schroer, T. A., Szilak, I., Steuer, E. R., Sheetz, M. P., and Cleveland, D. W. (1991) *J. Cell Biol.* **115,** 1639–1650
8. Schroer, T. A., and Sheetz, M. P. (1991) *J. Cell Biol.* **115,** 1309–1318
9. Karki, S., and Holzbaur, E. L. (1995) *J. Biol. Chem.* **270,** 28806–28811
10. Vaughan, K. T., and Vallee, R. B. (1995) *J. Cell Biol.* **131,** 1507–1516
11. Waterman-Storer, C. M., Karki, S., and Holzbaur, E. L. (1995) *Proc. Natl. Acad. Sci. U.S.A.* **92,** 1634–1638
12. Waterman-Storer, C. M., Karki, S. B., Kuznetsov, S. A., Tabb, J. S., Weiss, D. G., Langford, G. M., and Holzbaur, E. L. (1997) *Proc. Natl. Acad. Sci. U.S.A.* **94,** 12180–12185
13. Kimura, N., Imamura, O., Ono, F., and Terao, K. (2007) *J. Neurosci. Res.* **85,** 2909–2916
14. Moos, T. (1995) *Brain Res.* **672,** 14–23
15. De Lacalle, S., Cooper, J. D., Svendsen, C. N., Dunnett, S. B., and Sofroniew, M. V. (1996) *Neuroscience* **75,** 19–27
16. Niewiadomska, G., and Baksalerska-Pazera, M. (2003) *Neuroreport* **14,** 1701–1706
17. Niewiadomska, G., Baksalerska-Pazera, M., and Riedel, G. (2005) *Ann. N.Y. Acad. Sci.* **1048,** 287–295
18. Kimura, N., Yanagisawa, K., Terao, K., Ono, F., Sakakibara, I., Ishii, Y., Kyuwa, S., and Yoshikawa, Y. (2005) *Neuropathol. Appl. Neurobiol.* **31,** 170–180
19. Tamai, Y., Kojima, H., Ohtani, Y., Uchida, K., Taguchi, F., Kawaguchi, T., Miura, S., and Tateishi, J. (1989) *Microbiol. Immunol.* **33,** 35–42
20. Kimura, N., Nakamura, S. I., Honda, T., Takashima, A., Nakayama, H., Ono, F., Sakakibara, I., Doi, K., Kawamura, S., and Yoshikawa, Y. (2001) *Brain Res.* **922,** 30–41
21. Ida, N., Hartmann, T., Pantel, J., Schröder, J., Zerfass, R., Förstl, H., Sandbrink, R., Masters, C. L., and Beyreuther, K. (1996) *J. Biol. Chem.* **271,** 22908–22914
22. Nakamura, S., Nakayama, H., Goto, N., Ono, F., Sakakibara, I., and Yoshikawa, Y. (1998) *J. Med. Primatol.* **27,** 244–252
23. Kimura, N., Tanemura, K., Nakamura, S., Takashima, A., Ono, F., Sakakibara, I., Ishii, Y., Kyuwa, S., and Yoshikawa, Y. (2003) *Biochem. Biophys. Res. Commun.* **310,** 303–311
24. Jordens, I., Marsman, M., Kuijl, C., and Neefjes, J. (2005) *Traffic* **6,** 1070–1077
25. Caviston, J. P., Ross, J. L., Antony, S. M., Tokito, M., and Holzbaur, E. L. (2007) *Proc. Natl. Acad. Sci. U.S.A.* **104,** 10045–10050
26. Brady, S. T. (1985) *Nature* **317,** 73–75
27. Riggs, B., Fasulo, B., Royou, A., Mische, S., Cao, J., Hays, T. S., and Sullivan, W. (2007) *Mol. Biol. Cell* **18,** 3313–3322
28. Traer, C. J., Rutherford, A. C., Palmer, K. J., Wassmer, T., Oakley, J., Attar, N., Carlton, J. G., Kremerskothen, J., Stephens, D. J., and Cullen, P. J. (2007) *Nat. Cell Biol.* **9,** 1370–1380
29. Lippincott-Schwartz, J., and Fambrough, D. M. (1987) *Cell* **49,** 669–677
30. Allan, V. (1996) *Curr. Biol.* **6,** 630–633
31. Holleran, E. A., Karki, S., and Holzbaur, E. L. (1998) *Int. Rev. Cytol.* **182,** 69–109
32. Martin, M., Iyadurai, S. J., Gassman, A., Gindhart, J. G., Jr., Hays, T. S., and Saxton, W. M. (1999) *Mol. Biol. Cell* **10,** 3717–3728
33. Deacon, S. W., Serpinskaya, A. S., Vaughan, P. S., Lopez, Fanarraga, M., Vernos, I., Vaughan, K. T., and Gelfand, V. I. (2003) *J. Cell Biol.* **160,** 297–301
34. Schroer, T. A. (2004) *Annu. Rev. Cell Dev. Biol.* **20,** 759–779
35. Welte, M. A. (2004) *Curr. Biol.* **14,** R525–R537
36. Esch, F. S., Keim, P. S., Beattie, E. C., Blacher, R. W., Culwell, A. R., Oltersdorf, T., McClure, D., and Ward, P. J. (1990) *Science* **248,** 1122–1124
37. Wang, R., Meschia, J. F., Cotter, R. J., and Sisodia, S. S. (1991) *J. Biol. Chem.* **266,** 16960–16964
38. Cataldo, A. M., Mathews, P. M., Boiteau, A. B., Hassinger, L. C., Peterhoff, C. M., Jiang, Y., Mullaney, K., Neve, R. L., Gruenberg, J., and Nixon, R. A. (2008) *Am. J. Pathol.* **173,** 370–384
39. Aniento, F., Emans, N., Griffiths, G., and Gruenberg, J. (1993) *J. Cell Biol.* **123,** 1373–1387
40. Valetti, C., Wetzel, D. M., Schrader, M., Hasbani, M. J., Gill, S. R., Kreis, T. E., and Schroer, T. A. (1999) *Mol. Biol. Cell* **10,** 4107–4120
41. Jordens, I., Fernandez-Borja, M., Marsman, M., Dusseljee, S., Janssen, L., Calafat, J., Janssen, H., Wubbolts, R., and Neefjes, J. (2001) *Curr. Biol.* **11,** 1680–1685
42. Driskell, O. J., Mironov, A., Allan, V. J., and Woodman, P. G. (2007) *Nature Cell Biol.* **9,** 113–120
43. Lebrand, C., Corti, M., Goodson, H., Cosson, P., Cavalli, V., Mayran, N., Fauré, J., and Gruenberg, J. (2002) *EMBO J.* **21,** 1289–1300
44. Harrison, R. E., Bucci, C., Vieira, O. V., Schroer, T. A., and Grinstein, S. (2003) *Mol. Cell. Biol.* **23,** 6494–6506
45. Russo, R., Borghi, R., Markesbery, W., Tabaton, M., and Piccini, A. (2005) *FEBS Lett.* **579,** 6027–6030
46. Sharples, R. A., Vella, L. J., Nisbet, R. M., Naylor, R., Perez, K., Barnham, K. J., Masters, C. L., and Hill, A. F. (2008) *FASEB J.* **22,** 1469–1478
47. Kokubo, H., Saido, T. C., Iwata, N., Helms, J. B., Shinohara, R., and Yamaguchi, H. (2005) *Neurobiol. Aging* **26,** 409–418
48. Rajendran, L., Honsho, M., Zahn, T. R., Keller, P., Geiger, K. D., Verkade, P., and Simons, K. (2006) *Proc. Natl. Acad. Sci. U.S.A.* **103,** 11172–11177
49. Trojanowski, J. Q., and Mattson, M. P. (2003) *Neuromolecular Med.* **4,** 1–6
50. Forman, M. S., Trojanowski, J. Q., and Lee, V. M. (2004) *Nat. Med.* **10,** 1055–1063
51. Norris, E. H., Giasson, B. I., and Lee, V. M. (2004) *Curr. Top. Dev. Biol.* **60,** 17–54
52. Lin, S. X., Ferro, K. L., and Collins, C. A. (1994) *J. Cell Biol.* **127,** 1009–1019
53. Runnegar, M. T., Wei, X., and Hamm-Alvarez, S. F. (1999) *Biochem. J.* **342,** 1–6
54. Norris, C. M., Halpain, S., and Foster, T. C. (1998) *J. Neurophysiol.* **80,** 1567–1570
55. Jiang, C. H., Tsien, J. Z., Schultz, P. G., and Hu, Y. (2001) *Proc. Natl. Acad.*

Sci. U.S.A. **98,** 1930–1934
56. Jouvenceau, A., and Dutar, P. (2006) *J. Physiol. Paris* **99,** 154–161
57. Gong, C. X., Singh, T. J., Grundke-Iqbal, I., and Iqbal, K. (1993) *J. Neurochem.* **61,** 921–927
58. Gong, C. X., Shaikh, S., Wang, J. Z., Zaidi, T., Grundke-Iqbal, I., and Iqbal, K. (1995) *J. Neurochem.* **65,** 732–738
59. Ladner, C. J., Czech, J., Maurice, J., Lorens, S. A., and Lee, J. M. (1996) *J. Neuropathol. Exp. Neurol.* **55,** 924–931
60. Vogelsberg-Ragaglia, V., Schuck, T., Trojanowski, J. Q., and Lee, V. M. (2001) *Exp. Neurol.* **168,** 402–412
61. Tanimukai, H., Grundke-Iqbal, I., and Iqbal, K. (2005) *Am. J. Pathol.* **166,** 1761–1771
62. Grundke-Iqbal, I., Iqbal, K., Tung, Y. C., Quinlan, M., Wisniewski, H. M., and Binder, L. I. (1986) *Proc. Natl. Acad. Sci. U.S.A.* **83,** 4913–4917
63. Yoon, S. Y., Choi, J. E., Choi, J. M., and Kim, D. H. (2008) *Neurosci. Lett.* **437,** 111–115
64. Ravikumar, B., Vacher, C., Berger, Z., Davies, J. E., Luo, S., Oroz, L. G., Scaravilli, F., Easton, D. F., Duden, R., O'Kane, C. J., and Rubinsztein, D. C. (2004) *Nat. Genet.* **36,** 585–595
65. Ravikumar, B., Acevedo-Arozena, A., Imarisio, S., Berger, Z., Vacher, C., O'Kane, C. J., Brown, S. D., and Rubinsztein, D. C. (2005) *Nat. Genet.* **37,** 771–776
66. Fader, C. M., Sánchez, D., Furlán, M., and Colombo, M. I. (2008) *Traffic* **9,** 230–250

Arch Environ Contam Toxicol
DOI 10.1007/s00244-009-9421-9

Enhanced Inhibitory Effects of TBT Chloride on the Development of F_1 Rats

H. Asakawa · M. Tsunoda · T. Kaido · M. Hosokawa · C. Sugaya · Y. Inoue · Y. Kudo · T. Satoh · H. Katagiri · H. Akita · M. Saji · M. Wakasa · T. Negishi · T. Tashiro · Y. Aizawa

Received: 26 March 2009 / Accepted: 3 November 2009

Abstract Neurotoxicity is one of the major effects of tributyltin (TBT). The effects on the next generation of F_1 rats exposed to TBT via the placenta and their dams' milk may be stronger than those on adults. Pregnant Wister rats were exposed to TBT at 0 and 125 ppm in their food. Half of the female F_1 rats in both groups were exposed to TBT at 125 ppm in their food from 9 to 15 weeks of age. Female F_1 rats were divided into the following groups: the control-control (CC) group, with no exposure; the TBT-control (TC) group, exposed to TBT via the placenta and their dams' milk; the control-TBT (CT) group, exposed to TBT via their food from 9 to 15 weeks of age; and the TBT-TBT (TT) group, exposed to TBT via the placenta, their dams' milk, and their food ($n = 10$/group). After administration, an open-field test and prepulse inhibition (PPI) test were performed at 15 weeks of age. The mean body weights of the TC and TT groups were significantly lower than that of the CC group from 9 to 15 weeks of age. The mean relative thymus weight of the TC and TT groups was significantly lower than that of the CC group. In the open-field test, a marked decrease in the total locomotion distance was observed in the TT group. The mean values in the TT and TC groups were significantly lower than that in the CC group. For the locomotion distance between 15 and 20 min, the mean values in the CT, TC, and TT groups were significantly lower than that in the CC group. The mean locomotor distance between 25 and 30 min in the TT group was significantly lower than that in the CC and TC groups. The mean values of instances of wall rearing in the TC, CT, and TT groups were significantly lower than that in the CC group. The mean value of face washing or body washing in the TT group was significantly lower than that in the CT group. There were no significant differences in indexes of the PPI test. Exposure to TBT via the placenta and their dams' milk inhibited the development of F_1 rats, which continued after weaning. Inhibition of the rats' activity induced by exposure to TBT via the placenta and their dams' milk and/or via their food was suggested. The effects were most evident in the TT group.

H. Asakawa · M. Tsunoda (✉) · T. Kaido · M. Hosokawa · C. Sugaya · Y. Inoue · Y. Kudo · Y. Aizawa
Department of Preventive Medicine and Public Health, Kitasato University School of Medicine, 1-15-1 Kitasato, Sagamihara, Kanagawa 228-8555, Japan
e-mail: mtsunoda@med.kitasato-u.ac.jp

H. Asakawa · H. Katagiri
Department of Public Health, Kitasato University School of Allied Health Sciences, Sagamihara, Kanagawa, Japan

T. Satoh
Kitasato Clinical Research Center, Kitasato University School of Medicine, Sagamihara, Kanagawa, Japan

H. Akita · M. Saji
Department of Physiology, Kitasato University School of Allied Health Sciences, Sagamihara, Kanagawa, Japan

M. Wakasa · T. Negishi · T. Tashiro
Aoyama Gakuin University School of Science and Engineering, Sagamihara, Kanagawa, Japan

Tributyltin (TBT) compounds have been widely used as biocides and antifouling agents (Boyer 1989; Arakawa 2000). Restrictions on the application of TBT as a vessel antifouling agent were introduced in 1990 (Horiguchi 1998); however, TBT pollution in fish and shellfish has been and is still being reported worldwide (Ueno et al. 2004; Mizuishi et al. 2005; Meng et al. 2009).

Humans are exposed to TBT via the ingestion of TBT-contaminated fish and shellfish. There are few studies estimating the daily intake of TBT. Tsuda et al. (1995)

Published online: 25 November 2009

estimated the daily intake of TBT from meals as 4.7 μg in 1991 and 2.2 μg in 1992. The tentatively acceptable daily intake (ADI) of TBT oxide compiled by the Ministry of Health and Welfare in Japan at that time was 1.6 μg/kg body weight (Morita 1991). The daily intake of TBT is likely to be considerably lower than the ADI. Tsunoda (1993) also concluded that the exposure level to TBT from the contamination in Niigata, Japan, is not likely to be at a critical level by comparing actual TBT levels in fish and shellfish and the ADI. It should be noted that the ADI was decided for adults.

Neurotoxicity, as well as immunotoxicity, is one of the major toxic effects of TBT (Boyer 1989; Arakawa 2000). Especially, it is suggested that the neurotoxic effects from exposure to TBT via the placenta and their dams' milk in mice are stronger than those in adult mice from exposure via their food (Tsunoda et al. 2006; Konno et al. 2005) as well as immunotoxicity (Kimura et al. 2005). Fetuses and infants are exposed to TBT via the placenta and their dams' milk. Whether or not such exposure induces developmental neurotoxicity has not been elucidated. For example, it is not clear whether enhanced neurotoxic effects on the F_1 generation are found in animals other than mice. In addition, it is of interest whether or not the effects of TBT on the central nervous system remain after the cessation of exposure via the placenta and their dams' milk after weaning. The cessation of exposure clarifies the difference among effects via the placenta, their dams' milk, and their food.

Although the method for evaluation of the neurotoxicity of animals exposed to toxicants during their development has not yet been established, the open-field test (Kobayashi et al. 2004), a behavioral test, has been used for evaluation of neurotoxicity in animals as a screening test. In addition to the open-field test, the prepulse inhibition (PPI) test (Inada et al. 2003) is known as one of the representative tests for screening of neurotoxicity. Locomotor activity and behaviors in adaptive response to a novel environment are evaluated by the open-field test, and functions of learning and cognition are evaluated by the PPI test. Aou et al. (2000) reported the neurotoxic effects on F_1 rats using the open-field test and other behavioral tests, in which F_1 rats were continuously exposed to TBT via the placenta, their dams' milk, and their food. Effects of cessation of exposure to TBT during development have not been reported.

The objective of this study was to elucidate the developmental neurotoxicity of TBT. Pregnant rats were given TBT chloride in their diet. The offspring were exposed to TBT via the placenta and their dams' milk. Exposure was stopped 3 weeks after delivery (at weaning). After development, half of the F_1 rats were again exposed to TBT via their food. Comparing groups, we tried to elucidate the effects of TBT via the placenta, their dam's milk, or their food.

Materials and Methods

Experimental Animals and Treatment

Wistar rats, 9 weeks of age and pregnant for the first time (Oriental Bioservice, Tokyo), were administered 0 and 125 ppm of TBT chloride in their food ($n = 4$ for the control, $n = 6$ for TBT-exposed groups) in polycarbonate shoebox-style cages. Rodent chow containing TBT was prepared by Oriental Bioservice. Rats were given free access to food and tap water. The daily intake of food and water was recorded by the time of delivery. The number of F_1 rats for each dam was recorded. After weaning, dams were euthanized, and the implantations for each rat were counted by observing the uterus.

Exposure to TBT in F_1 rats was stopped 3 weeks after delivery (the weaning time). After weaning, the F_1 rats were fed with a commercially available rodent chow. At 9 weeks of age, female F_1 rats were again randomly assigned to the control group or the treatment groups. Treatment groups were fed a diet containing 125 ppm of TBT chloride from 9 to 15 weeks of age. F_1 rats were divided into the following four groups: the control-control (CC) group, with no exposure; the TBT-control (TC) group, exposed to TBT via the placenta and their dams' milk; the control-TBT (CT) group, exposed to TBT via their food oral from 9 to 15 weeks of age; and the TBT-TBT (TT) group, exposed to TBT via the placenta, their dams' milk, and their food ($n = 10$/group) (Fig. 1). Two F_1 rats from each group were maintained in a cage and ate and drank ad libitum at 22°C and 45% humidity, with a 14/10-h light/dark cycle. From 9 to 15 weeks of age, the body weight and the intake of food and water were recorded

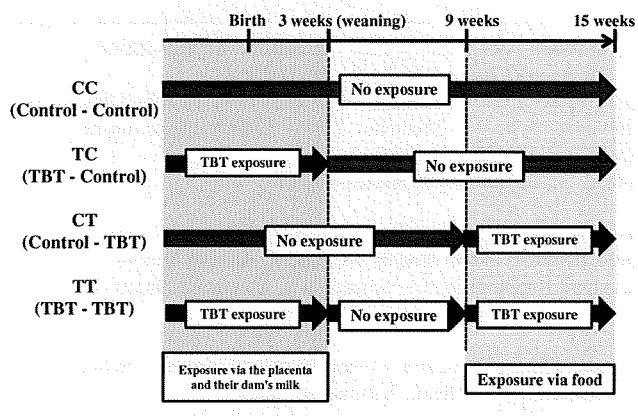

Fig. 1 Protocol for TBT exposure to female F_1 rats. TBT exposure via the placenta and their dams' milk: pregnant rats were exposed to TBT chloride via their food, which contained 125 ppm of TBT chloride, i.e., their offspring were exposed to TBT chloride via the placenta and their dams' milk. TBT exposure via food: female F_1 rats were exposed to TBT chloride via food that contained 125 ppm of TBT chloride